ARCHIVES OF ELECTRICAL ENGINEERING VOL. 68(3), pp. 497–510 (2019)

DOI 10.24425/aee.2019.129337

A novel method for separability of signal components to estimate radiation from a high-frequency subsystem

MILAD DANESHVAR[1], NASER PARHIZGAR[1], HOMAYOON ORAIZI[2]

[1]*Department of Electrical Engineering, Shiraz branch*
Islamic Azad University
Shiraz, Iran
email: naserpar@yahoo.com

[2]*Department of Electrical and Computer Engineering*
Iran University of Science and Technology
Tehran, Iran

(Received: 22.09.2018, revised: 04.03.2019)

Abstract: Specific requirements are designed and implemented in electronic and telecommunication systems for received signals, especially high-frequency ones, to examine and control the signal radiation. However, as a serious drawback, no special requirements are considered for the transmitted signals from a subsystem. Different industries have always been struggling with electromagnetic interferences affecting their electronic and telecommunication systems and imposing significant costs. It is thus necessary to specifically investigate this problem as every device is continuously exposed to interferences. Signal processing allows for the decomposition of a signal to its different components to simulate each component. Radiation control has its specific complexities in systems, requiring necessary measures from the very beginning of the design. This study attempted to determine the highest radiation from a subsystem by estimating the radiation fields. The study goal was to investigate the level of radiations received and transmitted from the adjacent systems, respectively, and present methods for control and eliminate the existing radiations. The proposed approach employs an algorithm which is based on multi-component signals, defect, and the radiation shield used in the subsystem. The algorithm flowchart focuses on the separation and of signal components and electromagnetic interference reduction. In this algorithm, the detection process is carried out at the bounds of each component, after which the separation process is performed in the vicinity of the different bounds. The proposed method works based on the Fourier transform of impulse functions for signal components decomposition that was employed to develop an algorithm for separation of the components of the signals input to the subsystem.

Key words: electromagnetic interference, electromagnetic radiation, parameter estimation, multi-component signals, frequency response, radio frequency

1. Introduction

Today's systems are all affected by electromagnetic interferences one way or another. In the past, systems operated at frequencies no higher than a few megahertz (MHz), and their efficiency was not affected by the configuration of elements and tracks and their interconnections. However, today, new phenomena are likely to occur considering the increase in system frequencies up to a few gigahertz (GHz), such that inappropriate system design and lack of knowledge on the respective principles in this regard can easily cause interference in the system performance [1, 2].

Appropriate design measures have to be taken to control the radiations in a system that consists of the printed circuit board (PCB) and electronic components on the subsystem subject to electromagnetic interference. Radiation is among the most common interferences negatively affecting the systems and interfering with their performance. Different specialized approaches obtained both experimentally and theoretically, have been presented by numerous researchers to reduce the electromagnetic interferences (EMIs) [3, 4].

The most prominent experience in this regard is to reduce the order of the transmission line models. This method is one of the ways. For example, a mixed potential integral equation (MPIE) is the model for EMI reduction. This method can be implemented by considering the number of independent variables [5].

The idea of creating parametric modeling in reducing the order of the transmission line is not a new method. Recently proposed methods have been developed to focus on the static functions of the subject, but the applied purpose is to analyze the parametric modeling of multi-component signals by improving the signal quality and reducing the order of transmission lines. Creating any parametric model with the assumption that any electrical behavior of the elements in the system can be modeled by a variable dynamic system in the time domain, also has the ability to run for nonlinear systems [6–8]. However, this approach has been less concerned with the new components that are added to the signals and affect the system behavior. Measures have to be taken in the design of printed circuit boards (PCBs) to control and eliminate radiation. To this end, the present study aimed to determine a radiation coefficient in high-frequency systems subject to the effect of odd harmonics [9, 10]. The components' separation of a signal expresses an important task in multi-component signal applications.

In the initial state without any hypothesis, the signal is analytic and mono-component. In signal analytic methods, we use mono-component signals to demonstrate non-stationary and nonlinear signals rather than the Fourier transform solutions, such as functions used in empirical method decomposition. A mono-component signal has non-negative instantaneous frequencies. It is a real-valued signal model of finite energy that is defined as the derivative of the signal phase function. In practice, the simulations result in showing which signals appear depending on the different type of environmental conditions. The challenge ahead is for multi-component signals that produce different results inaccurate simulations.

For this reason, the accurate analysis of signals in time and frequency domains is necessary [11]. For multi-component signals, a method focused on the decomposition of signal components into a single component is considered.

In the signal analysis, the general transforms from the time domain to the frequency spectrum can display a large amount of energy consumed by noise in multi-component signals [1, 12]. Practical experiments are demonstrated to illustrate the general computation [13–16]. In the

PCB simulation, a 3 mm spacing was considered between the adjacent traces, and the traces were assumed to be 12 cm long. Given the 9 mm width assumed for traces and their aerial spacing of 2 mm and the proposed amount of Hyper Lynx software simulation performances, the circuit impedance was considered $Z = 133\ \Omega$, and the subsystem interference was calculated at a frequency of 80 megahertz (MHz). In this case, the capacitance effect of each trace was represented by C_{11} and C_{22}, while that of the adjacent traces with C_{12}. The capacitive effect of each trace is calculated using Equation (1):

$$C_{11} = C_{12} = \frac{0.12 \times 2\pi \times \varepsilon}{\cosh^{-1}\left(\frac{0.3}{0.9}\right)} = 3.5\ \text{pF}, \tag{1}$$

where $\varepsilon = 8.85 \times 10^{-12}$. The capacitance effect between every two adjacent traces is expressed by:

$$C_{12} = \frac{0.12 \times \pi \times \varepsilon}{\cosh^{-1}\left(\frac{2}{1.8}\right)} = 7.1\ \text{pF}. \tag{2}$$

The impedances of capacitors C_{11} and C_{22} at a frequency of 80 MHz are identical and equal to 569 Ω. The parallel impedance between the load and supply is considered important and, therefore, is regarded an important factor in the calculations of capacitor C_{12}. Reducing the capacity of this capacitor can reduce the interference to a great extent. Moreover, moving the traces away from each other is another way of reducing interference, in which case, increasing the traces spacing from 2 to 3 mm reduces the capacitive effect from 7.1 pF to 5.03 pF, consequently decreasing the interference down to 4 dB. The capacitive coupling impedance is greater than the impedance of the subsystem and hence may not be neglected in the calculations. By employing Equation (3), the total interference can be calculated from Equation (3) as follows:

$$P_{\text{int}12} = 20 \log \left| \frac{vl_1}{vl_2} \right| = 20 \log \left| \frac{10 \parallel 133}{10 \parallel 133 + j569} \right| = -34\ \text{dB}. \tag{3}$$

The two following simulations are considered for radiation estimation. In the first simulation, the radiation field is estimated. The frequency in this scenario was considered 80 MHz, which corresponds to a wavelength of 3.75 m. The load impedance was considered 500 Ω, which is greater than the impedance of the free space (377 Ω). Therefore, the maximum magnitude of the electric field is calculated as follows:

$$|E|_{\max} \approx \frac{(1.7v) \times (0.05 \times 0.02\ \text{m}) \times \left(\frac{2\pi}{3.75\ \text{m}}\right)^2}{4\pi \times (3\ \text{m})} \approx 126.6\ \mu\text{V/m}\ [42.04\ \text{dB}]. \tag{4}$$

According to the federal communication commission (FCC) standard for the acceptance of class B, the field factor is 100 μV/m and in dB is 40 dB, which magnitude of an electric field is 2.04 dB greater than the standard margin. In the second simulation, in order to deal with the problem in Simulation 1, impedance estimation was carried out in a subsystem with a lower impedance. The load impedance was initially selected lower than that of the free space (377 Ω). At a frequency of 80 MHz, the corresponding load impedance was considered 33 Ω, which

is a common value in software simulations. In fact, the ground layer of the circuit exhibits an inductive effect, preventing us from accurately calculating the radiative effect while taking into account the inductive effect. Therefore, the electric field can only be approximately estimated.

$$|E|_{\max} \approx \frac{(1.7v) \times (0.05 \times 0.02 \text{ m}) \times \left(\frac{2\pi}{3.75 \text{ m}}\right)^2}{4\pi \times (3 \text{ m})} \left(\frac{377}{|50 + j33|}\right) \approx 597.5 \text{ μV/m [55.5 dB]}.$$

By assuming a semi-radiative ground path, the semi-radiative value can be considered 5 dB, resulting in a total of 60.5 dB by considering the above-calculated value. According to the FCC standard in the considered interval, this subsystem is within the acceptable radiation range as Class B [17, 18]. The input impedance and radiative resistance can be defined in small-sized subsystems due to the voltage generated at the two terminals of the voltage source in the case of an open-circuit output voltage along with a time-varying current in a conductor. Power loss and radiative power are, respectively, calculated as follows:

$$P_{\text{loss}} = \frac{1}{2} |l_i|^2 R_{\text{loss}} \approx \frac{1}{2} \left| \frac{v_i}{R_{\text{loss}} + jwL} \right|^2 R_{\text{loss}} = \frac{1}{2} \times \left| \frac{1.8}{569} \right|^2 \times 569 = 2.8 \text{ mW}, \tag{5}$$

$$P_{Emiss} = \frac{1}{2} \times \frac{|E|^2}{377} = \frac{1}{2} \times \frac{\left|129 \times 10^{-6}\right|^2}{377} = 22 \text{ pW/m}^2. \tag{6}$$

The amount of radiation power in all directions can be as follows:

$$P_{Emiss} < P_{Emiss} \times (4\pi r^2) = (22 \times 10^{-12}) \times (4\pi) \times (2)^2 = 1.1 \text{ nW}. \tag{7}$$

Therefore, the radiation coefficient of the field can be calculated according to Equation (8).

$$E_M < \frac{1.1 \times 10^{-9}}{1.1 \times 10^{-9} + 2.8 \times 10^{-3}} = 3.9 \times 10^{-7} = 0.000039\%. \tag{8}$$

At low frequencies, the input impedance is usually a function of the frequency of the input signal, i.e. $Z_i \approx 1/(2\pi f c)$. However, it should be noted that further frequency decrease can lead to negative impedances. The maximum radiation can be obtained at a 2 m distance from the antenna. The maximum radiative power is calculated as follows:

$$P_{Emiss\,\max} = \frac{P_{Emiss}}{4\pi r^2} d_i = \frac{22 \times 10^{-12}}{4\pi \times (2)^2} \times (2.41) = 1.05 \text{ pW/m}^2, \tag{9}$$

where $P_{Emiss}/(4\pi r^2)$ is the mean power density and $d_i = 2.41$ is the distance from the radiation location. The highest radiation of the electric field is calculated from Equation (10):

$$|E_{Emiss\,\max}| = \sqrt{2 Z_e P_{Emiss}} = \sqrt{2 \times 377 \times (1.05 \times 10^{-12})} = 28.1 \text{ μv/m}. \tag{10}$$

The comparison between the magnitudes of the electric fields obtained in the above calculations suggests that the trace size is not important in the calculations. Therefore, based on these calculations, the radiative efficiency is obtained as follows:

$$\eta = \frac{28.1 \text{ μv/m}}{126.6 \text{ μv/m}} = 0.22 = -13.15 \text{ dB}. \tag{11}$$

Radiation control in modern digital systems is as difficult as the design of the digital logic itself. Therefore, appropriate measures have to be taken from the very beginning of the design. The rise time and fall time of the signal input to the subsystem were, respectively, 0.6 s, and 80 MHz in the simulations. Hence, the initial and secondary objectives were to determine the main frequency of the input signal and calculate the amplitude of the odd harmonics, respectively. The signal period was 50 ns, by which the central frequency can be calculated as follows:

$$F_0 = \frac{1}{T} = \frac{1}{5 \times 10^{-8}} = 20\ \text{MHz}. \tag{12}$$

By employing Equation (12):

$$2\,|C_n| = \frac{2 \times m_t}{T} \times \left| \frac{\sin\left(\frac{n\pi\tau}{T}\right)}{\left(\frac{n\pi\tau}{T}\right)} \right| \times \left| \frac{\sin\left(\frac{n\pi t_r}{T}\right)}{\left(\frac{n\pi t_r}{T}\right)} \right|. \tag{13}$$

Each of the odd harmonics (1, 3, 5, 7, 11), has values of 0.356–0.118–0.07–0.05 and 0.03, respectively, and with changes observed in the harmonic range is affected by the rise time, since a reduction can be observed in the amplitude by applying these changes. The extent of changes can be calculated as follows:

$$V = 20 \log \frac{\left| \frac{\sin\left(\frac{n\pi\tau}{T}\right)}{\left(\frac{n\pi\tau}{T}\right)} \right|}{2\,|C_n|}. \tag{14}$$

The odd harmonics (1, 3, 5, 7, 11), have change rates of 8.05, 8.1, 8.13, 8.17, and 8.34 in dB, respectively. The above calculations indicate that changes in the rise time can significantly affect higher harmonics without tangibly affecting the signal shape. Therefore, regarding the interference in frequencies with high harmonics, the shape of the digital signal can be modified by the addition of rising time to control the radiation.

The rest of this paper is organized as follows; in section 2, the proposed algorithm is introduced. Simulation results and measurement of the signal are presented in section 3. Conclusions are made in section 4.

2. The proposed algorithm

Identifying the different radiative components of a subsystem is a problem to be tackled from multiple aspects. This study aimed to achieve a comprehensive algorithm for identification of radiation sources. Matrix $\boldsymbol{M}$ indicates a full set of the available test methods for identifying the existing radiations. The parameters m and n addresses the number of methods, and the vector values $\boldsymbol{C}$ and $\boldsymbol{T}$ denote the cost and time of tests.

Test Method $\boldsymbol{M} = [M_1\ M_2\ \ldots\ M_m]^T, \quad M_i \in \{0,1\} = \{\text{absent, present}\},$

Test Cost $\boldsymbol{C} = [C_1\ C_2\ \ldots\ C_m]^T \quad \text{and} \quad \sum_{i=1}^{m} c_i = 100,$

Test Time $\boldsymbol{T} = [t_1\ t_2\ \ldots\ t_m]^T \quad \text{and} \quad \sum_{i=1}^{m} t_i = 100,$

Radiated Defects $\boldsymbol{D} = [D_1\ D_2\ \ldots\ D_n]^T,$

Application Risks $\boldsymbol{AR} = [AR_1\ AR_2\ \ldots\ AR_5]^T,$
AR_1: Critical, AR_2: High, AR_3: Medium, AR_4: Low, AR_5: Very Low,

Percent-Radiated Component $\boldsymbol{PRC} = [p_1\ p_2\ \ldots\ p_7]^T,$
$p_1 : EMI,\ p_2 : EFT,\ p_3 : EMP,\ p_4 : ESD,\ p_5 : RFI,\ p_6 : RE,\ p_7 : CE,$

Defect Radiated Matrix $\boldsymbol{CD} = \begin{bmatrix} d_{11} & d_{12} & \cdots & d_{17} \\ d_{21} & d_{22} & \cdots & d_{27} \\ \vdots & \vdots & \ddots & \vdots \\ d_{n1} & d_{n2} & \cdots & d_{n7} \end{bmatrix}, \quad d_{ij} \in \{0,1\} = \{\text{absent present}\},$

Defect Frequency $\boldsymbol{DF} = \boldsymbol{CD} * \boldsymbol{PCC}^T,$

Target Defect $\boldsymbol{DC} = [DC_1, DC_2, \ldots, DC_n]^T,$

Confidence Level $= \boldsymbol{AR}[i] * \boldsymbol{DF}.$

The following relations can be used for identification of the radiation source, upgrading the system security equipment, and implementing the EMI reduction requirements [11]. It was assumed that the cost and time of all radiation identification methods were fixed. The matrix $\boldsymbol{X}$ is considered as random input according to Equation (15):

$$\boldsymbol{X} = \begin{pmatrix} x_{11} & x_{12} & \cdots & x_{1n} \\ x_{21} & x_{22} & \cdots & x_{2n} \\ \vdots & \vdots & \ddots & \vdots \\ x_{m1} & x_{m2} & \cdots & x_{mn} \end{pmatrix}. \tag{15}$$

In this matrix, the columns (1, 2, ..., n) and rows (1, 2, ..., m) represent the absence and presence of signals exposed to radiation. Each input matrix $\boldsymbol{X}$ indicates the ability to identify radiation. In case two or more identification methods are considered, these relations are expressed using Equation (16):

$$X_{Emissj} = 1 - \prod_{i=1}^{m_i} \left(1 - x_{ij}\right) \quad \text{for detection of } j, \tag{16}$$

where m_i denotes the number of methods in the test set. This test method has high importance in the assessment of effectiveness. Using radiation shielding, this can assess all the damages caused by radiation defect in the subsystem and the controlled radiation. In Figure 1, we show the flowchart of the research methodology, which fully describes the steps of the proposed method.

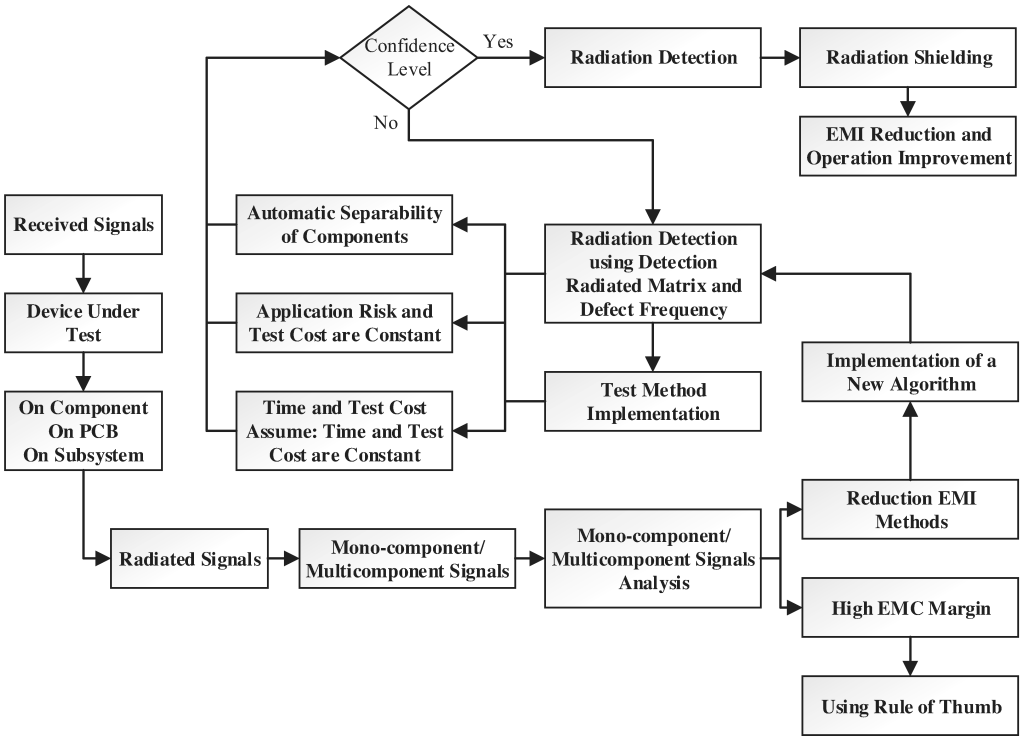

Fig. 1. Flowchart of the research methodology

The algorithm initializes the set under testing, after which the priority in the arrangement of variables can be studied based on the independent variable of the process and by calculating the frequency and radiation level. The signals entering the subsystem are commonly modeled using a set of combined components with low amplitude and frequency variations. Therefore, separation of the components in a signal is the main focus of many problems related to subsystem processes with various applications. The most common methods for automatic separation of components use signals based on time and time-frequency units. The proposed method works based on the Fourier transform of impulse functions for signal components decomposition. The Fourier transform of signals is represented by $\hat{s}$, and the normalization process for the aforementioned function is defined as follows:

$$\hat{s}(\varepsilon) = \int_R s(x) e^{-2i\pi\varepsilon x} D_x \,. \tag{17}$$

For $s \in L^2(R)$, the continuous transform for a signal is defined as follows:

$$P_s(b,\tau) = \int_R s(x) \frac{1}{b} \overline{\xi\left(\frac{x-\tau}{b}\right)} D_x \,, \tag{18}$$

where $s \in L^2(R)$ satisfies the condition:

$$\int_0^{+\infty} \frac{\left|\hat{\xi}(\varepsilon)\right|}{\varepsilon} D_\varepsilon < +\infty,$$

which is considered an analytical equation, given that $\hat{\xi}(\varepsilon) = 0, \varepsilon \leq 0$.

By denoting the highest frequency domain unit by ε_ξ, an experimental class of analytical signals is employed through the following definition:

$$\varepsilon_\xi = \arg\max_{\varepsilon} \left|\hat{\xi}(\varepsilon)\right|. \tag{19}$$

In this section, the effort was made to separate the signal components using the s_k components of a multi-component signal. The function for signals is defined as follows:

$$s(\tau) = \sum_{k=1}^{K} m_k(\tau) \cos\left(2\pi\varphi_k(t)\right) = \sum_{k=1}^{K} s_k(\tau),$$

where $m_k(\tau) > 0$ and $\varphi_k'(\tau) > 0$. Note that separation of signal components, implementation, and determining the operational frequency results in a systematic procedure which can be demonstrated in the following pattern:

$$\{PL\}_l^\infty = 0 \;\Rightarrow\; p_l = \left[\frac{p_l + p_{l-1}}{2}, \frac{p_l + p_{l+1}}{2}\right].$$

In fact, the performance of $S^\beta_{S,\widetilde{\in}}$ can be approximated as:

$$T_s(p_l, \tau) = \int_{b:|\hat{p}(b,\tau)\in p_l|} P_s(b, \tau) \frac{D_b}{b},$$

such that the following function is satisfied:

$$s(\tau) = \frac{2}{H\varsigma} \mathrm{Re}\left[\sum_l T_s(p_l, \tau)\right].$$

Using the change of variables technique, it can be inferred that:

$$T_s(p_l, \tau) = \int_{u:\left|\hat{p}\left(2^{u/n_v}\Delta\tau, \tau\right)\right| \in p_l} P_s\left(2^{u/n_v}\Delta\tau, \tau\right) \frac{\log 2}{n_v} D_u,$$

where the distribution of units can be expressed as follows:

$$b_j = 2^{j/n_v}\Delta\tau, \quad j = 0, \ldots, L_{n_v} - 1.$$

There, the term $\Delta\tau$ denotes the transient time slope.

By assuming $n_b = L_{n_v}$, the highest frequency is obtained as:

$$\bar{p} = p_{n_b-1} = \frac{1}{2\Delta\tau}$$

and assuming an alternative signal, the lowest signal value is calculated as:

$$\frac{1}{T} = \frac{1}{n\Delta\tau} = p_0 = \underline{p} \quad \text{(note that } T = n\Delta\tau\text{)}.$$

Considering the variations in p are defined in a logarithmic scale as $pl = 2^{l\Delta p}\underline{p}$, the variations in the angle of the signal input to the subsystem can be finally calculated as follows:

$$\Delta p = \frac{1}{n_b - 1}\log_2\frac{n}{2}.$$

Ultimately, it can be concluded that for an appropriate coefficient of time interval variation, the main period of the main function is obtained as follows:

$$T_{D,s}(p_l, q) = \sum_{0\le j\le n_b-1,\ j:\left|\hat{p}(b_j,q\Delta\tau)\right|\in p_\tau} p_s(b_j, q\Delta\tau)\frac{\log 2}{n_b}.$$

The above operator yields:

$$s(q\Delta\tau) \approx \frac{2}{H_v}\mathrm{Re}\left[\sum_l T_{D,s}(p, q)\right].$$

As a matter of fact, separability in multi-component signals is a process which is based on operators. Therefore, looking for a particular state in the time-frequency domain should be such that the highest level of energy is provided.

$$\left(H_q^*\right) = 0, \ldots, n-1.$$

The total changes made in this case can be realized by calculating the following quantity.

$$H^* = \underset{h\in\{0,\ldots,n_b-1\}}{\arg\max}\sum_{q=0}^{n-1}\log\left(\left|T_{D,s}\left(ph_q, q\right)\right|^2\right) - \sum_{q=0}^{n-1}\lambda\Delta p\left|h_q - h_{q-1}\right|^2.$$

Given the complexity of the problem, an approximation of H^* is simply sufficient to complete the investigation results. We use the obtained equations for entry angle computation, in the study of the multi-component signal.

Consider the expression:

$$s(\tau) = \sum_{k=1}^{K} m_k(\tau)\cos\left(2\pi\varphi_k(\tau)\right),$$

such that the following approximation is yielded:

$$p_s(m, \tau) \approx \sum_{k=1}^{K}\frac{1}{2}me^{2i\pi\varphi\tau}\,\overline{Z(m\varphi)}. \tag{20}$$

This approximation can also be reformulated as:

$$\in \left(\widetilde{H}_1(s_i)_{i=1,\ldots,K}\right) I_1 + \left(\widetilde{H}_2(s_i)_{i=1,\ldots,K}\right) I_2 + \left(\widetilde{H}_3(s_i)_{i=1,\ldots,K}\right) I_3\,,$$

where $\widetilde{H}_i$ is not dependent on the type of the selected algorithm, or in other words, this level of approximation is not dependent on the selected signal type. Therefore, based on the previous studies, a single-frequency signal with a small approximation Δ experiences a high level of variations. Hence, the effort was made to sufficiently separate each component from the rest of components so that for each $(m,\ \tau)$, Equation (20) is simplified such that the following relation is correctly expressed:

$$\frac{\varepsilon_z + \Delta}{\varphi'_k(\tau)} < \frac{\varepsilon_z - \Delta}{\varphi'_{k-1}(\tau)} \quad \Leftrightarrow \quad \frac{\Delta}{\varepsilon_z} < \frac{\varphi'_k(\tau) - \varphi'_{k-1}(\tau)}{\varphi'_k(\tau) + \varphi'_{k-1}(\tau)}\,.$$

In our calculations, we may conclude that in the above inequality holds true as long as the following relation holds true:

$$\Delta \leq \varepsilon_z D.$$

The above conditions include the vector sum of the two cosine functions with two close frequencies as well as the sum of two linear functions with two close instantaneous frequencies, such that both the existing signals satisfy the following conditions:

$$\varphi'_1(\tau) - \varphi'_2(\tau) = \frac{1}{10}\left(\varphi'_1(\tau) + \varphi'_2(\tau)\right).$$

These signals can be analyzed using an impulse by taking into account the two following conditions:

$$\varepsilon_\varsigma = \mu = 1, \qquad \Delta = \sigma.$$

In each case, a second-degree function is associated with two signals of the same phase. The resulting functions can be associated with an acceptable approximation of variable K.

$$\frac{\varepsilon_Z^2}{\left|\varphi'_K(\tau)\right|} \cdot \frac{\left|m''_k(\tau)\right|}{|m_k(\tau)|} \ll 1, \qquad \varepsilon_z^2 \cdot \frac{\left|\varphi''_k(\tau)\right|}{\left|\varphi'_k(\tau)\right|^2} \ll 1. \tag{21}$$

Given the inequality:

$$\frac{\varepsilon_Z^2}{\left|\varphi'_K(\tau)\right|} \cdot \frac{\left|m'_k(\tau)\right|}{|m_k(\tau)|} \leq 1,$$

the second-degree function can be obtained at a final value of Δk.

In the initial stage for determination of input signal threshold to the subsystem, the different possible scenarios in the separation of signal components are determined:

$$S_0(\tau) = \{\gamma \in \Gamma(\tau),\ s,\ \tau(H_s(\gamma, \tau)) = N_s\}\,.$$

By defining T_0 at times T associated with $S_0(\tau)$, we may calculate the threshold $\hat{\gamma}(\tau)$ based on T at T_0. The result is as follows:

$$\hat{\gamma}(\tau) = \text{median}(S_0(\tau)).$$

Given the value τ, $S_0(\tau)$ is generated such that the condition $m \to |P_s(m, \tau)|$, at the smallest N_s value reach its highest value, and the term $\gamma(\tau)$ assumes its appropriate value.

3. Simulation and measurement of the signal

The radiation of the subsystem was tested, and the results were registered in the respective logs. We suggest looking into the peak detection code written in MATLAB based on the algorithm flowchart for separation of multi-component signals. This algorithm carries out the detection algorithm at the bounds of each component and then reconstructs the components by employing the information in the vicinity of the different interval bounds.

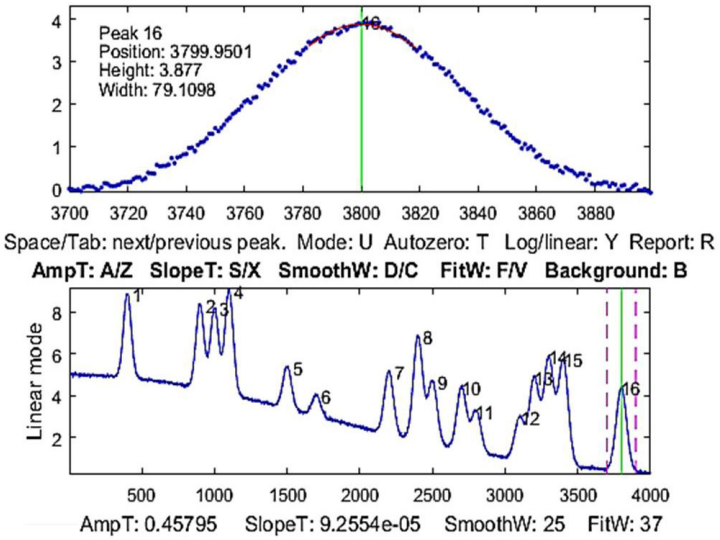

Fig. 2. The number of counted peaks in the signal input to the subsystem

In Table 1, radiation is measured in 5 states. In order to investigate the performance of the subsystems subject to the radiation effects, the tests in Table 2 were conducted on the subsystem, and the results were registered.

Table 1. Experimental measurement of subsystem radiation

Location ID	Status	Unit	Min	Max	RMS	Pk	Overload
Ch1	Enabled	dB	−29.37796	29.03437	18.26644	29.37796	No

Signal Plot Points: 2048	**Initial Drive (V):** 0.005	**Drive Limit (V Pk):** 2
Sweep Type: Logarithmic	**Compression Rate:** Fast	**Bandwidth (%):** 25
Measurement Strategy: Proportional Filter	**Ramp Rate:** Slow	**Abort Sensitivity:** 0.50

In the test condition using start frequency 9 KHz, stop frequency 40 MHz and input amplitude −13 dBm by steps 10 ms, and according to Table 2, we measure the frequency response of the subsystem. The interference of adjacent signals and control of radiation in subsystems subject to different ambient conditions are investigated in the Figures 3 and 4, and the result of the measurement is desirable.

Table 2. Results of frequency response test conducted on the system

Output Amplitude Max.	−13.22 dBm
Frequency of Amplitude Max.	3.51 MHZ
Cut off Frecuency −3 dBm	20.88 MHZ

Test type: VCS (Swept Sine), Sweeping Rate: 1 Oct/Min, Sweep Number: 63, Frequency: 686.9 Hz, **Signal Plot Points:** 2048, **Sweep Type:** Logarithmic.

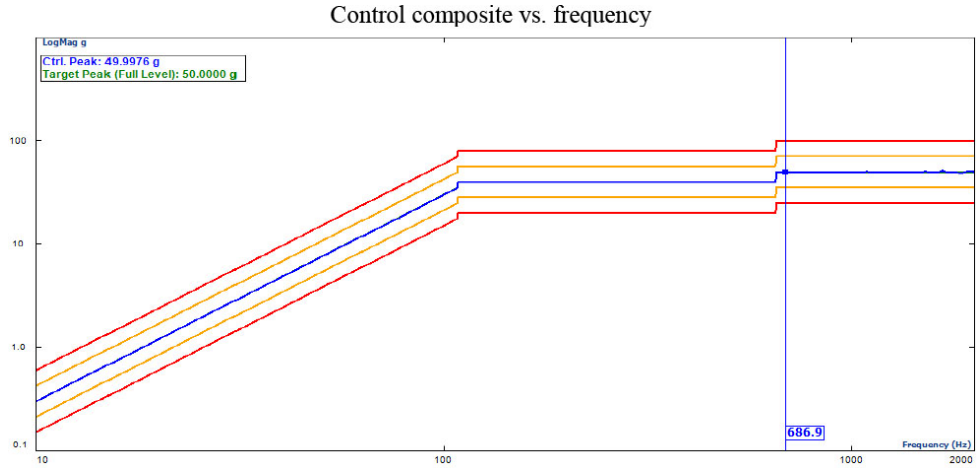

Fig. 3. Subsystem radiation control

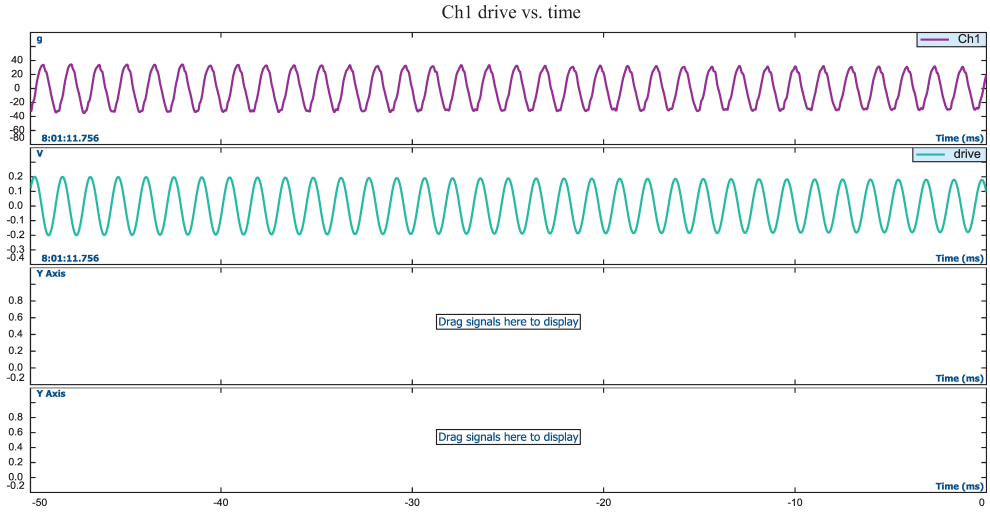

Fig. 4. Interference of adjacent signals in radiative mode

4. Conclusion

The present study aimed to determine a radiation coefficient in high-frequency systems subject to the effect of odd harmonics. Moreover, a new method for separation of the components in a high-frequency signal and identification of radiation defect was presented.

The algorithm initializes the set under testing, after which the priority in the arrangement of variables can be studied based on the independent variable of the process and by calculating the frequency and radiation level. Then, the structure of the Fourier transform was employed to develop an algorithm for separation of the components of the signals input to the subsystem to model a set of combined components with low amplitude and frequency variations. The subsystem was experimentally tested, and the results were registered in the respective test logs for a more accurate analysis of the signals entering the subsystem.

Using past experiences in system design based on specific principles, they can act to separate the signal components as accurately as possible. In fact, separability in multi-component signals is a process which is based on operators. Therefore, separation of the components in a signal is the main focus of many problems related to subsystem processes with various applications.

The most common methods for automatic separation of components use signals based on time and time-frequency units. The proposed method works based on the Fourier transform of impulse functions for signal components decomposition.

References

[1] Espejel-García D. *et al*., *An alternative vehicle counting tool using the Kalman filter within MATLAB*, Civil Engineering Journal, vol. 4, no. 3, pp. 1029–1035 (2017), DOI: 10.28991/cej-030935.

[2] Javadi K., Komjani N., *Investigation into Low SAR PIFA Antenna and Design a Very Low SAR U-slot Antenna using Frequency Selective Surface for cell-phones and Wearable Applications*, Italian Journal of Science and Engineering, vol. 1, no. 3, pp. 145–157 (2017), DOI: 10.28991/ijse-01117.

[3] Duan X., Rimolo-Donadio R., Brüns H.D., Schuster C., *Fast and Concurrent Simulations for SI, PI, and EMI Analysis of Multilayer Printed Circuit Boards*, Asia-Pacific Symposium on Electrom. Compatibility (APEMC), Beijing, China (2010), DOI: 10.1109/APEMC.2010.5475683.

[4] Li H., Li L., Tang Y.Y., *Mono-Component Decomposition of Signals Based on Blaschke Basis*, International Journal of Wavelets, Multiresolution and Information Processing, vol. 5, no. 6, pp. 941–956 (2007), DOI: 10.1142/S0219691307002130.

[5] Astaneh A.A., Gheisari S., *Review and Comparison of Routing Metrics in Cognitive Radio Networks*, Emerging Science Journal, vol. 2, no. 4, pp. 191–201 (2018), DOI: 10.28991/esj-2018-01143.

[6] Rasilainen K., Ilvonen J., Viikari V., *Antenna matching at harmonic frequencies to complex load impedance*, IEEE Antennas and Wireless Propagation Letters, vol. 14, pp. 535–538 (2015), DOI: 10.1109/LAWP.2014.2370760.

[7] Chia Hao K., Chang Fa Y., *Measurement and mitigation of electromagnetic interference from a radio navigation station to nearby power and telephone lines*, IEEE Transactions on Power Delivery, vol. 21, no. 4, pp. 2017–2021 (2006), DOI: 10.1109/TPWRD.2006.874571.

[8] Abhari R., Eleftheriades G.V., *Metallo-dielectric electromagnetic bandgap structures for suppression and isolation of the parallel-plate noise in high-speed circuits*, IEEE Transactions on Microwave Theory and Technique, vol. 51, no. 6, pp. 1629–1639 (2003), DOI: 10.1109/TMTT.2003.812555.

[9] Lundstedt H., Persson T., Andersson V., *The extreme solar storm of May 1921: observations and a complex topological model*, Annales Geophysicae, vol. 33, pp. 109–116 (2015), DOI: 10.5194/angeo-33-109-2015.

[10] Qiuhui C., Luoqing L., Wang Y., *Amplitudes of mono-component signals and the generalized sampling functions*, Signal Processing, vol. 94, pp. 255–263 (2014), DOI: 10.1016/j.sigpro.2013.06.034.

[11] Flamarz Al-Arkawazi S.A., *Measuring the Influences and Impacts of Signalized Intersection Delay Reduction on the Fuel Consumption, Operation Cost and Exhaust Emissions*, Civil Engineering Journal, vol. 4, no. 3, pp. 552–571 (2018), DOI: 10.28991/cej-0309115.

[12] Movahedian Attar N., *Dynamic Detection of Secure Routes in Ad hoc Networks*, Emerging Science Journal, vol. 1, no. 4, pp. 233–238 (2017), DOI: 10.28991/ijse-01127.

[13] Cats O., Jenelius E., *Planning for the Unexpected: The Value for Reserve Capacity for Public Transport Network Robustness*, Transportation Research Part A: Policy and Practice (2015), DOI: 10.1016/j.tra.2015.02.013.

[14] Kamgaing T., Ramahi O.M., *A novel power plane with integrated simultaneous switching noise mitigation capability using high impedance surface*, IEEE Microwave and Wireless Components Letters, vol. 13, no. 1, pp. 21–23 (2003), DOI: 10.1109/LMWC.2002.807713.

[15] Pushpendra S., Shiv D.J., Rakesh K.P., Kaushik S., *Fourier decomposition method for nonlinear and non-stationary time series analysis*, Processing in Mathematical, Physical and engineering sciences, vol. 473, no. 2199, pp. 1–27 (2017), DOI: 10.1098/rspa.2016.0871.

[16] ITU, *High-power electromagnetic immunity guide for telecommunication systems*, ITU-T, K.81 (2015), http://handle.itu.int/11.1002/1000/11830.

[17] Schuster C., *Ensuring Signal and Power Integrity for High-Speed Digital Systems*, IEEE 5th International Conference on Consumer Electronics, Berlin, Germany (2016), DOI: 10.1109/ICCE-Berlin.2015.7391234.

[18] Radasky W., Bäckström M., *Brief Historical Review and Bibliography of Intentional Electromagnetic Interference (IEMI)*, Beijing, China: URSI General Assembly (2014), DOI: 10.1109/URSI-GASS.2014.6929517.